IOP Publishing Nanotechnology
Nanotechnology 27 (2016) 205703 (10pp) doi:10.1088/0957-4484/27/20/205703

Real-space measurement of potential distribution in PECVD ONO electrets by Kelvin probe force microscopy

F Emmerich and C Thielemann

University of Applied Sciences Aschaffenburg, Biomems Lab—Department of Engineering, Aschaffenburg, 63741, Germany

E-mail: christiane.thielemann@h-ab.de

Received 28 July 2015, revised 12 February 2016
Accepted for publication 29 February 2016
Published 7 April 2016

Abstract

Multilayers of silicon oxide/silicon nitride/silicon oxide (ONO) are known for their good electret properties due to deep energy traps near the material interfaces, facilitating charge storage. However, measurement of the space charge distribution in such multilayers is a challenge for conventional methods if layer thickness dimensions shrink below 1 μm. In this paper, we propose an atomic force microscope based method to determine charge distributions in ONO layers with spatial resolution below 100 nm. By applying Kelvin probe force microscopy (KPFM) on freshly cleaved, corona-charged multilayers, the surface potential is measured directly along the z-axis and across the interfaces. This new method gives insights into charge distribution and charge movement in inorganic electrets with a high spatial resolution.

Keywords: electret, multilayer, charge distribution, Kelvin probe force microscopy

(Some figures may appear in colour only in the online journal)

1. Introduction

A detailed understanding of charge storage mechanisms is crucial for the evaluation of the long-term stability of electrets. In particular, multilayers of inorganic electrets are known for their excellent charge storage capabilities [1]. Although thermic ageing gives a good estimate of the electret's lifetime, characteristics of charges can only be fully understood if observed with high spatial resolution. For the case of homogeneously charged electret layers, the charge centroid is typically estimated by a simple approximation. Assuming a parallel-plate capacitor setup, the distance d_0 between the surface and charge centroid is $d_0 = \varepsilon_0 \varepsilon_r V_S A/Q$, where V_S is the measured surface potential, A the area and Q the transferred charge during corona charging [2]. More sophisticated calculations and the application of elaborated experimental methods such as pressure pulse, laser induced pressure pulse, thermal pulse, electroacoustic methods or CV measurements help to find more accurate results for the charge centroid [3]. In particular, the application of very high measurement frequencies, short laser pulses and statistical methods improve the existing methods to achieve resolutions in the micro- to nanometre range [4–6]. Nevertheless, all these methods are based on assumptions concerning the material properties such as thickness, acoustic impedance or density, and only give results with limited spatial resolutions [7]. Furthermore, the stated methods are either not applicable to thin multilayers or to non-metallized electrets. Thus, these methods can be classified as indirect, as they rely on measured values that are not directly coupled to the charge distribution.

To overcome these limitations we propose the direct method of Kelvin probe force microscopy (KPFM) for real-space measurements of potential distributions under ambient conditions. There KPFM achieves a lateral resolution down to a few tens of nanometres [8], whereas in an ultrahigh-vacuum even sub-nanometre resolution is possible [9]. This makes it the most accurate tool for the measurement of stored charge distributions, being favoured over other electrical AFM-based methods, such as electrical force distance curves [10] or the application of Teflon modified tips [11]. Therefore, we suggest for the first time, the application of KPFM to locate

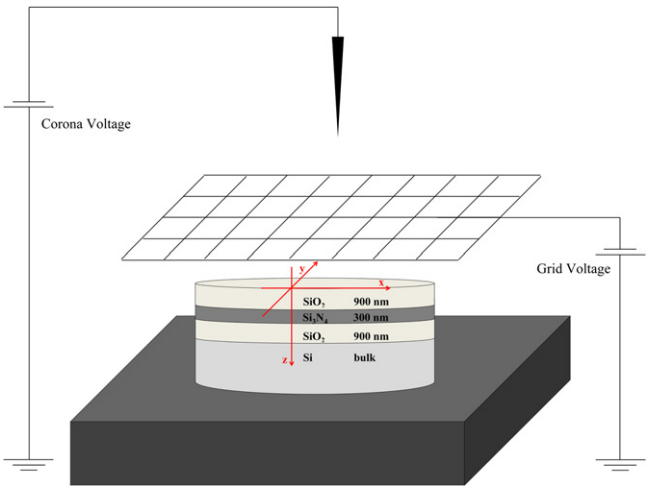

Figure 1. Schematic of the corona charging set-up with a grid to control the maximum surface potential. The coordinate system indicates the charging of the sample in the x–y plane.

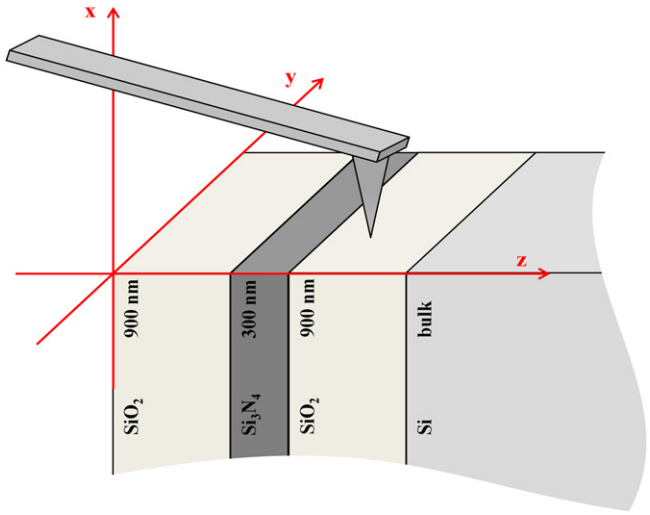

Figure 2. Measurement principle. The freshly cleaved sample is mounted in a vertical sample holder. KPFM measurements were performed along the z-axis of the ONO-multilayer.

charges along the z-axis of an inorganic multilayer electret system including three interfaces. So far, cross-sectional KPFM has found only limited applications. Several studies have been dedicated to the evaluation of the function of solar cells [12–16]. The high spatial resolution of KPFM allowed testing the devices during illumination. Further research is focused on the characterization of electrochemical etching processes [17].

As a model system we employ the well-known multilayer stack of corona-charged silicon oxide/silicon nitride/silicon oxide (ONO). Finally, with the help of Poisson's equations and comparison to finite element method (FEM) results, we extrapolate from the measured potential to the charge distribution, which allows us to qualitatively predict the movement of charges inside the multilayer electret after a thermal treatment. The characterization of this new method shall contribute to a better understanding of charge storage mechanisms in multilayer systems.

2. Materials and methods

Layers of 900 nm SiO_2, 300 nm Si_3N_4 and 900 nm SiO_2 were deposited onto highly p-doped ($+10^{18}\,cm^{-3}$) 100 mm $\langle 100 \rangle$ silicon wafers by plasma enhanced chemical vapour deposition (PECVD) (iX-Factory, Dortmund, Germany). As the resulting PECVD layers showed variations in height, especially in the border area, only the central part of the wafer (60 mm × 60 mm) was used for experiments. Wafers were diced in samples with an average size of 20 mm × 20 mm.

To achieve good electrical contact during charging, a 50 nm gold layer was sputtered onto the backside of all samples. Electret charging was performed with a conventional high-voltage corona charging set-up using a grid to control the surface potential [18], as illustrated in figure 1. A Heinzinger PNC-60000-1 (Heinzinger, Rosenheim, Germany) was used as the high voltage source.

After charging the electrets, measurements of surface potentials were conducted using a TREK 369 electrostatic voltmeter (TREK, New York, USA). For further analysis the surface potential was averaged ($n = 5$) over the sample area of 20 mm × 20 mm, with one position at each corner and one in the centre. The probe area of the voltmeter was 5 mm × 5 mm. Finally, charge drive-in was performed by thermal treatment in a Heraeus T5050EK (Heraeus, Hanau, Germany) convection oven.

Before measurements, the samples were cleaved resulting in an almost flat and uniform breaking edge along the z-axis, as illustrated in figure 2. This was done with a custom made set-up, as conventional methods like wafer dicing, laser cutting or polishing would have modified the surface potential of the breaking edge. Shortly after cleaving, the samples were mounted in a vertical AFM sample holder and measured along the z-axis using amplitude-modulation KPFM (AM-KPFM).

The following KPFM measurements were performed with an Asylum Research MFP-3D atomic force microscope (Asylum Research, Santa Barbara, USA) in lift mode using highly-doped silicon-tips PPP-NCH-R (Nanosensors, Neuchatel, Switzerland). These cantilevers had a typical tip-radius $\leqslant$7 nm, mean force constant of ~42 N m^{-1} and mean resonance frequency of ~330 kHz. During topography measurements in AC mode, the set-point was adjusted to achieve an average oscillation amplitude of ~80 nm, with a zero point of the tip ~40 nm above the surface. Delta height during lift mode KPFM was set to −10 nm, which resulted in a distance between tip apex and surface of approximately ~30 nm during the potential measurements. The tip voltage was adjusted to 0 V whereas the drive voltage was set to 3 V, representing a good compromise if topographic crosstalk shall be avoided. During all measurements the KPFM frequency was adjusted to the first mechanical resonance frequency and the scan speed was set to 1 μm s^{-1}.

3. Electret performance

Corona charging of the electrets was performed at room temperature under ambient condition. The corona voltage was set to −7.5 kV, whereas the grid voltage was adjusted to −200 V. As a result a maximum negative surface potential of about −140 V was achieved after 6 min, whereas 80% of the maximum surface potential was built-up within the first 2 min. Increasing the charging duration did not result in significantly higher surface potentials.

The surface potentials decayed to almost 0 V after 48 h, with a rapid decay during the first two hours (data not shown). This allows for two conclusions. Firstly, all charges are stored in shallow traps near the surface where they are easily removed through surface conductivity by isothermal decay [19]. Secondly, no charges are stored at the interfaces or the bulk of the oxide or nitride, aside from compensation charges at the silicon oxide/silicon interface attracted by the electric field.

In contrast to silicon oxide/silicon nitride double layers, where nitride acts as a hydrophobic top layer, PECVD ONO electrets do not perform very well without further treatment [20]. In order to improve the electret properties a hydrophobic surface modification with hexamethyldisilazane (HMDSN) was performed, which is known to increase the charge storage stability [20]. Before charging, samples were stored at 200 °C for 100 min to remove residual water molecules on the surface. Shortly after heating, the samples were placed in an evacuated exsiccator together with 50 ml of HMDSN for 24 h. Due to its low vapour pressure the liquid evaporates and forms a silane monolayer on the surface of the top silicon oxide. After corona charging, charge stability was significantly increased and after a decay of about 10% within the first 24 h surface potentials were stable for more than 6 months. All subsequent experiments were performed with HMDSN-treated samples as described above.

To evaluate the stability and temperature performance of the ONO layer, charge decay measurements at elevated temperatures between 50 °C and 300 °C were performed. No significant difference between samples stored at 50 °C and those stored at room temperature was observed. Even after 210 min the charge decay was less than 5%. In contrast, the surface potential decreased to almost 50% of its initial value after 210 min at 200 °C. At 300 °C the measured potential vanishes rapidly during the first hour and decreases to only 5% of its original value after only 210 min.

During heat treatment, thermic energy enables the loosely bound charge carriers to move inside the material. Here they either recombine with charges from the bulk material, travel deeper into the material, decay because of surface conductivity, or are trapped in deep energy traps. The latter case is especially relevant in the vicinity of interfaces [21]. As can be seen in figure 3, treatment at 300 °C results in an almost complete decay with only a small percentage of charge being left, stored in sufficiently deep traps. After a 200 °C treatment, the surface potential decreases to about 50%, what indicates that charges travel inside the material and presumably are stored near the material interfaces. Therefore, all samples for the KPFM measurements (see section 5) are treated at 200 °C for 200 min.

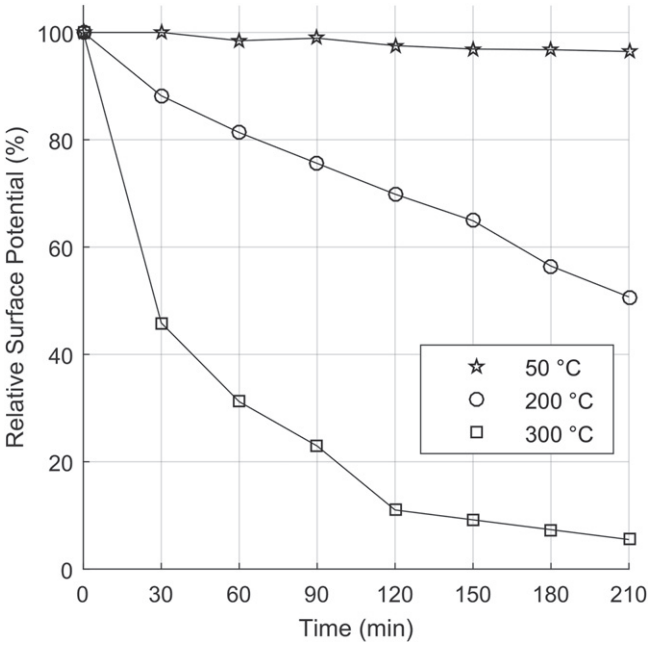

Figure 3. Relative surface potential of the ONO layers in the x–y plane plotted over time measured with an electrostatic voltmeter. Samples were stored at elevated temperatures. Up to 50 °C, the electrets show high stability, whereas at higher temperature the stability decreases. At 300 °C the surface potential vanishes almost completely after three hours ($n = 5$).

4. Modelling and simulation

As KPFM measures the electric potential on the surface of a sample, the charge distribution in the sample has to be derived from these measurement data. For this, theoretical considerations as well as FEM simulations were conducted on the multilayer system. After corona charging, introduced charges cause electric potentials inside the electret material which are described by the one-dimensional Poisson's equation. The relationship between charge, corresponding electric displacement, electric field, and the potential along the z-axis are shown in figure 4 for the ONO multilayer system (total thickness of 2100 nm) deposited on bulk silicon. For simplification, only negative charges on the silicon oxide surface ($z = 0$ nm) and compensation charges on the bulk surface ($z = 2100$ nm) are introduced. According to (1), the charges cause a constant electric displacement along the ONO multilayer, whereas the value of electric field depends on the relative permittivity ε_r.

The method of finite element modelling and simulation using the COMSOL Multiphysics electrostatics modules (Comsol Multiphysics, Germany) was employed to validate the hypothesis that the potential measured with KPFM around 30 nm above the sample is very close to the potential inside the electret material. For this purpose the multilayer system shown in figure 2 was modelled with the thicknesses given

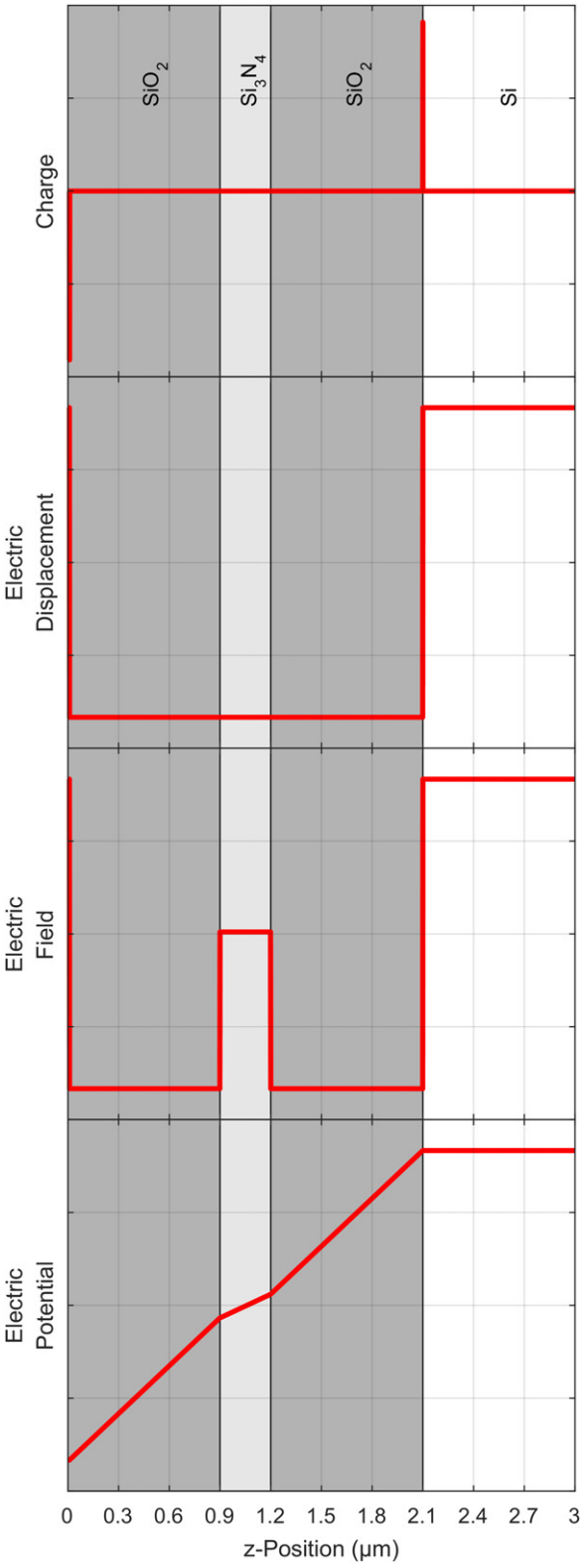

Figure 4. Correlation between (a) charge, (b) electric displacement, (c) electric field and (d) electric potential across a multilayer with different relative permittivities ε_r. The absolute value of the electric field is indirectly proportional to the permittivity of the material. Thus the electric potential, which represents, according to Poisson, the first derivative of the electric field, has a slope proportional to $1/\varepsilon_r$. As the bulk silicon is expected to behave like an ideal conductor, the electric displacement, electric field and potential inside the silicon are zero.

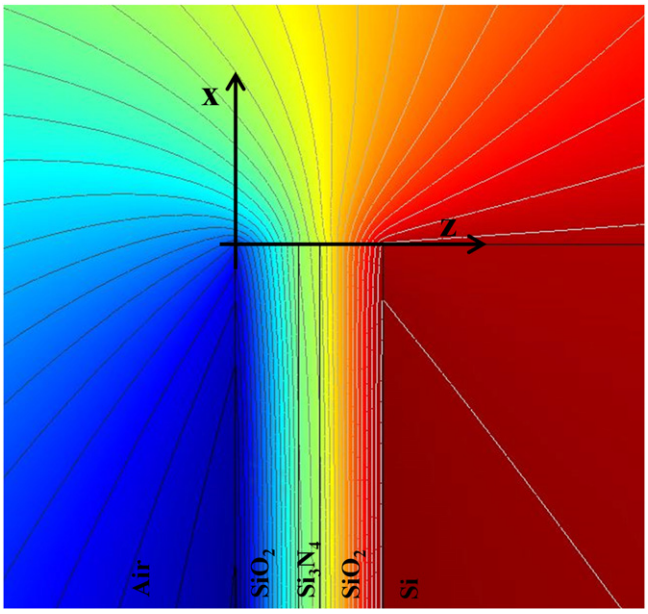

Figure 5. Qualitative FEM simulation of the potential inside the ONO layer and the surrounding air, with a surface charge of 2.5 mC m^{-2} at $z = 0$ nm. The bulk silicon ($z > 2100$ nm) (red) has a potential of almost 0 V, whereas the surface ($z = 0$ nm) of the top silicon oxide (blue) shows a potential of -5 V. With increasing z, the potential proceeds from -5 V (blue) to 0 V (red).

above. The relative permittivities ε_r of both silicon oxide layers were specified with 3.9, the silicon nitride layer with 7.5 and the surrounding air with 1.

Figure 5 shows a snippet of the simulated potential in the area of interest. The electrostatic field is generated by a surface charge density of 2.5 mC m^{-2} at $z = 0$ nm, which creates a compensation charge of opposite sign in the bulk silicon at $z = 2100$ nm. The value of charge density is chosen with the intention to approximate the range of measured potentials (see section 5). During the KPFM measurements the AFM tip is moved with a distinct distance of typically $x = 30$ nm along the z-axis. To achieve an accurate simulation in this plane, a partial mesh refinement, with mesh sizes smaller than 5 nm, was applied. To reduce computation time, fewer critical areas were simulated with larger mesh sizes up to 1000 nm.

A more quantitative result of the simulation is shown in figure 6. The distribution of the potential is plotted at different x-levels, where negative values represent a plane inside the sample and positive values a plane in the surrounding air. Clearly, the potential distribution in the multilayer electret with charges at the surface ($z = 0$ nm) and at the 'backside' (z = 2100 nm) can be described by a parallel-plate capacitor model with three dielectric layers. This results in a slope that is indirectly proportional to the different relative permittivities ε_r as shown by solving the one-dimensional Poisson's equation in its differential form

$$\nabla^2\phi(z) = -\nabla E(z) = -\rho(z)/(\varepsilon_0\varepsilon_r(z)), \qquad (1)$$

where $\phi(z)$ is the surface potential, $E(z)$ the electric field, $\rho(z)$ the charge density and ε_0 and ε_r the vacuum and relative permittivity, respectively (see also figure 4). Close to the

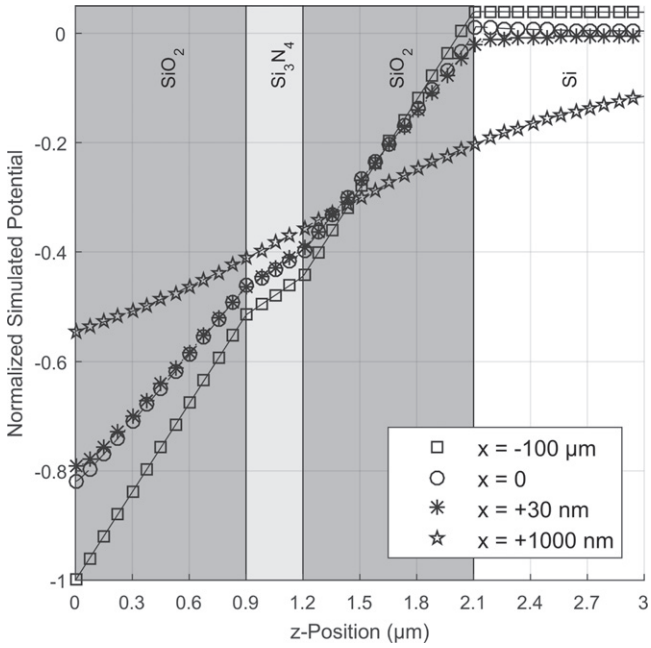

Figure 6. Cross-sections of the simulated potential as function of z at various x-positions (negative values for potentials inside the sample and positive values for potentials above in air) with surface charge density of 2.5 mC m^{-2} at $z = 0$ nm and compensation charges in the Si bulk at z = 2100 nm. The potential at the KPFM tip distance ($x = +30$ nm) is reasonably close to the actual potential inside the sample.

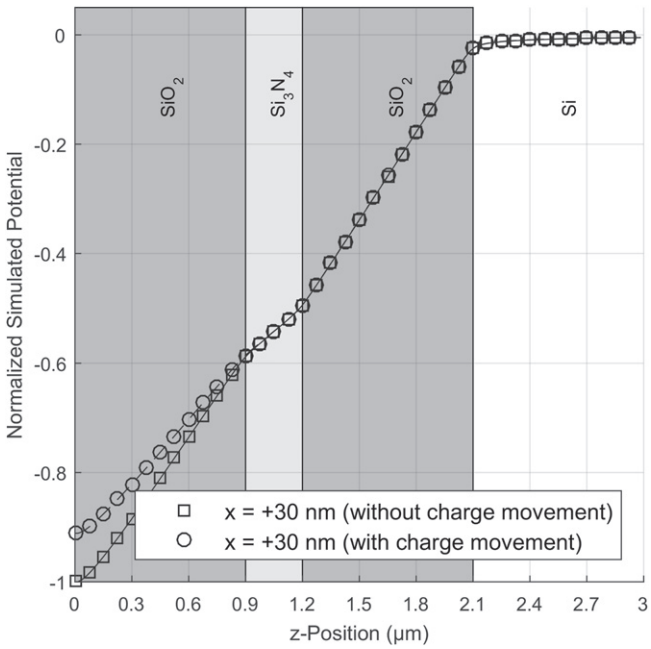

Figure 7. Cross-section of simulated potentials with and without charges trapped at the top oxide/nitride interface as function of z for $x = +30$ nm. Simulated surface charge densities were chosen to be 2.0 mC m^{-2} at $z = 0$ nm, 0.5 mC m^{-2} at z = 900 nm and compensation charges of -2.5 mC m^{-2} in the Si bulk at $z = 2100$ nm have been applied. The charge movement to the first interface results in a reduced slope of the potential inside the top oxide, whereas the slope in the nitride and the bottom oxide layers stay unaffected.

surface, inhomogeneity of the electric field occurs because of the transition from material to air. Deep inside the sample the field is homogeneous along the x-axis (see figure 5). This results in deviation of the potential between the surface and inside the sample ($x = -100$ μm). Consequently, the slope of the potential in the z-direction on and near the surface is slightly reduced, as compared to inside the material. The KPFM tip measuring position 30 nm above the surface, mirrors the actual potential inside the sample ($x = -100$ μm) sufficiently closely. Aside from dissimilar slopes in all three layers, the potential turns out to be smoothened only at intersections between the different electret materials. The overall error between the potential at the surface and 30 nm above is in the range of $\pm 2.5\%$, whereas at 1000 nm above the surface, subtle variations of the potential cannot be resolved anymore. Thus, it is crucial to apply the KPFM method, allowing for a small distance between surface and measuring tip. In conclusion, the potentials measured with the new KPFM method are a sufficiently exact mirror of the actual potential distribution inside the sample.

As already mentioned, charge storage in deep energy traps at the material interfaces is likely and has been described before [21]. For negative charges travelling from the top silicon oxide surface driven by thermal excitation into the layer system, capture at the nitride interface seems realistic, prohibiting further charge movement into the material. According to (1) this results in a decreased slope in the top material and a slightly reduced maximum potential.

To quantitatively describe the potential after thermal treatment at the KPFM measuring position, further simulations were performed. Therefore 0.5 mC m^{-2} of the initial negative charge at the silicon oxide/air interface was shifted to the top oxide/nitride interface, whereas the compensation charge in the bulk was kept at the same value. Comparative results with and without charge movement are depicted in figure 7, while values are normalized to the surface potential.

As illustrated in figure 7, charge movement decreases the slope in the top oxide layer as well as the maximum potential at the surface ($z = 0$ nm). The slopes inside the nitride and in the bottom oxide layers are unaffected by the movement of charges. Consequently, the slope of the potentials, especially the ratio between the slope in top and bottom oxide, leads to information about charge travelling inside the material and about the new position of these charges.

5. Measurements

Conventional AFM analysis was performed along the middle of the breaking edge of uncharged, freshly cleaved samples to determine possible interfering effects between topography and potential measurements. As the sample length of a few centimetres was very large compared to the 5 μm measurement length, dimensions in the y-direction are considered infinite.

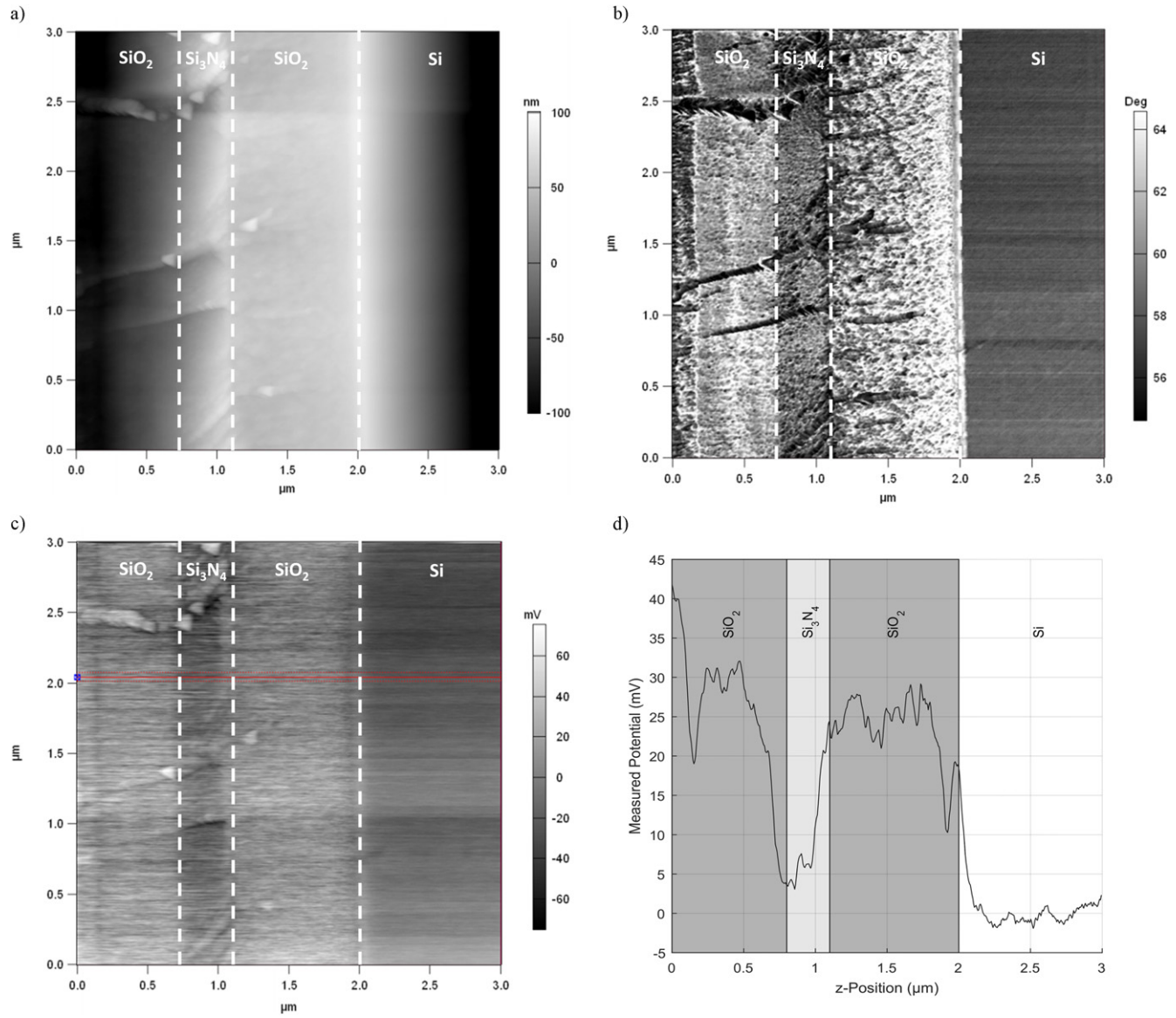

Figure 8. (a) AFM topography, (b) AFM phase image and (c) KPFM potential image of a freshly cleaved, uncharged sample. The phase image, revealing the four different materials, allows for identification of each layer and corresponding interfaces. The surface layer ($z < 0.2\ \mu$m) is a measurement artefact due to the tip passing over into air. (d) shows a cross-section of the potential image (c) indicated at the red line. The relative difference of up to 50 mV between the oxide/nitride layers and the bulk silicon may be introduced by the breaking process or due to different work functions of the sample materials.

As indicated in the measurement data in figure 8, the bulk silicon starts at 2000 nm, the bottom oxide layer ranges from 1100 to 2000 nm, the nitride layer from 800 to 1100 nm and the top silicon layer is cut off 100 nm in front of the actual surface. The crystalline bulk silicon is very smooth with a roughness R_a below 1 nm. In contrast, the multilayer of amorphous oxide and nitride is less smooth. The top and bottom silicon oxides show a roughness of <4 nm with a slight rise in height, whereas in the silicon nitride small islands appear, resulting in a roughness of up to 30 nm [22], as shown in figure 8(a). Topographic features, which are only visible in the ONO multilayer, are generated by the cleaving process, where the crystalline silicon breaks along a crystal-axis and the amorphous layers will break in an unpredictable way.

In addition, phase images were detected, indicating the phase-shift between excitation frequency and ensuing frequency of the cantilever. This signal is a very good indicator for material properties, such as stiffness, nano-roughness and different adhesion forces between sample and probe [23]. The three layers of the ONO system and the bulk silicon can clearly be distinguished in the phase image, allowing for a very precise determination of the interface locations as depicted in figure 8(b).

For calibration, KPFM measurements were firstly performed on uncharged samples, as can be seen in figures 8(c) and (d). Only small differences in surface potential of around 50 mV between bulk silicon and the multilayer were found, which were neglected in the further evaluation. These differences might be caused by the breaking procedure of the

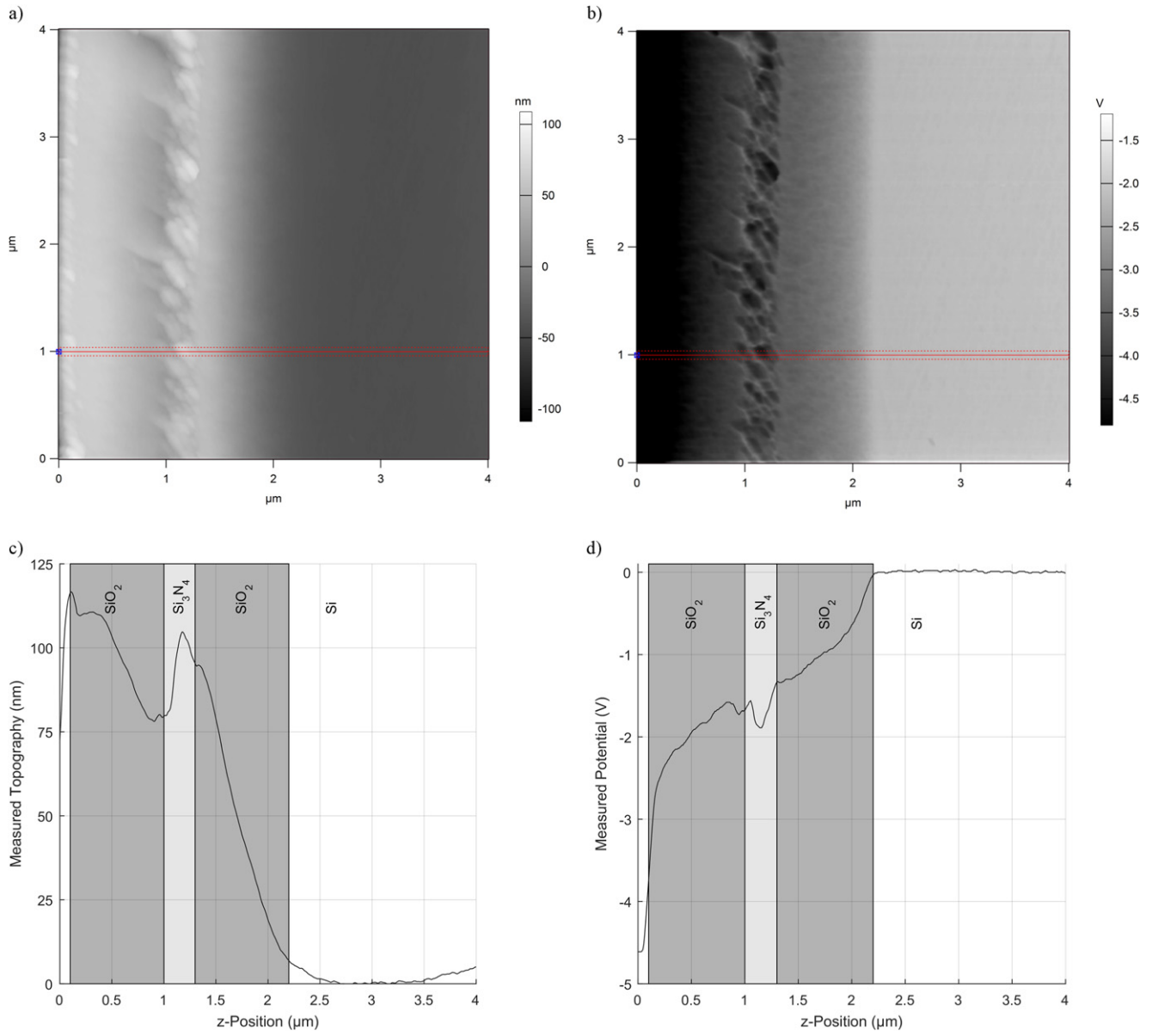

Figure 9. (a) AFM topography and (b) corresponding KPFM potential image of a freshly cleaved, charged and thermally treated sample. The roughness in the silicon nitride layer is also visible in the potential image, indicating possible topographic crosstalk. (c) Cross-section of the topography and (d) corresponding cross-section of the KPFM potential.

multilayer or due to different work functions of the sample materials.

When KPFM measurements were performed with charged samples, measurements revealed a potential distribution along the z-axis, clearly resembling the course of the simulated potentials in figure 6. As expected, the slopes of the potential along the z-axis inside both oxide layers were similar, whereas the slope inside the nitride layer was lower (results not shown). Near the surface, the potential dropped faster than predicted, probably due to the tip scanning the edge between sample and air, also visible in the phase image in figure 8.

Finally, measurements were performed on charged samples annealed at 200 °C for 200 min. As stated in section 3, the thermal treatment energizes the charges to travel through the material to be trapped near the interfaces. In figure 9 the AFM and KPFM measurements of such a sample are presented. Comparing figures 9(a) and (b), there is a clear indication for the topography of the nitride layer in the potential image. This topographic crosstalk is induced by the rough topography in the nitride domain, which can, in agreement with the literature, be explained by nano-roughness inside the nitride layer [24, 25]. The corresponding cross-sections in figures 9(c) and (d) show that the topographic crosstalk is only visible in the nitride layer, whereas the top and bottom oxide as well as the bulk are unaffected.

6. Discussion

As shown in section 4, the charge density is directly coupled to the second derivative of the potential and the permittivity

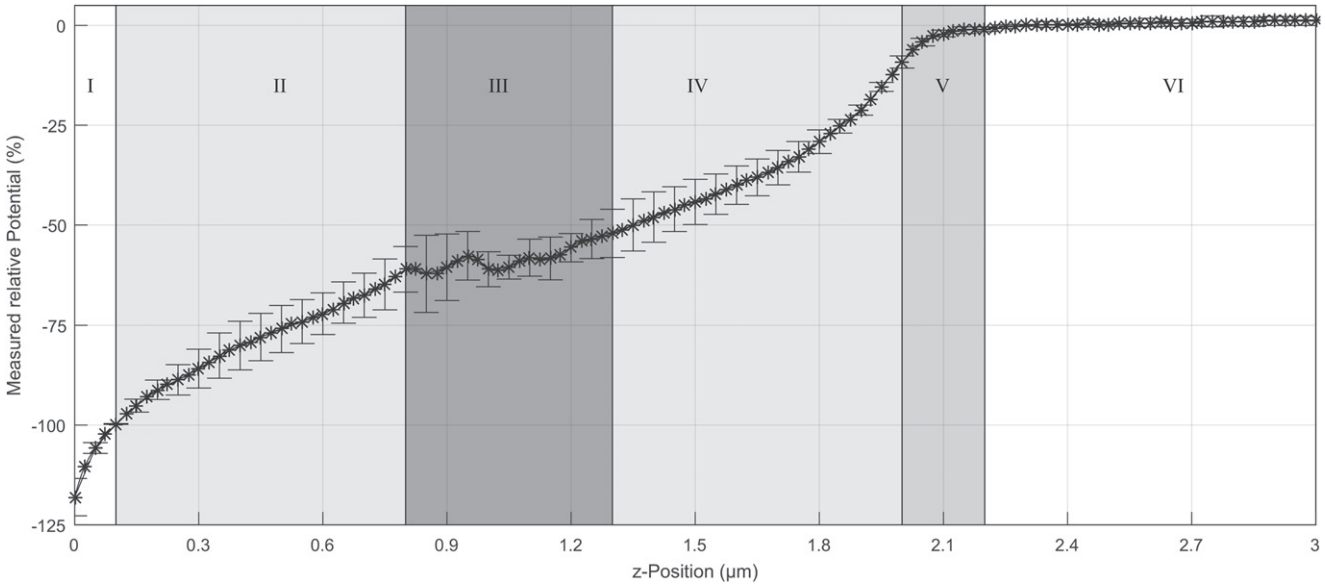

Figure 10. Arithmetic mean of KPFM measurement cross-sections on five equally treated samples (200 °C, 200 min) directly after cleaving. Major variations occur only in domain III, presumably caused by topographic crosstalk, and will be evaluated differently. For further discussion, the graph is divided into six domains, described in table 1.

Table 1. Different domains of the potential distribution in respect to the location in z-direction and material.

Domain	z-Coordinates	Material	Name
I	0–100 nm	Air/SiO_2	Edge area
II	100–800 nm	SiO_2	Top oxide layer
III	800–1300 nm	Si_3N_4	Nitride layer including transitions
IV	1300–2000 nm	SiO_2	Bottom oxide layer
V	2000–2200 nm	SiO_2/Si	Insulator/semiconductor transition
VI	2200–3000 nm	Si	Bulk silicon

of the material. Hence, the potential distribution depends on three parameters: the amount of induced charge, the permittivity, and the localization of charges in the dielectric material. Assuming thermal treatment does not affect permittivity, a change in the potential distribution can only be associated with a vanishing charge or a change in charge position. While the former only affects the maximum potential, a movement of charge into the z-direction of the material is related to a decrease of the potential's slope in the top layer. For the measured potential, six domains are identified, summarized in table 1, and depicted in figure 10.

To prove the validity of the method for multilayer systems, various samples were measured using KPFM. Figure 10 shows the arithmetic mean of potential cross-sections obtained from measurements on five equally treated samples. For better interpretability, the averaged values are normalized to the respective potential value at the beginning of domain II. It is clearly visible that domain II and domain IV follow a constant slope whereas domain III does not. As this crosstalk does not allow the direct analysis of this layer, in further discussion domain III will be evaluated differently to the top and bottom oxide.

Domain I, situated directly at the breaking edge, shows a steeper slope than the residual potential. However, this is not caused by a specific charge distribution but by measurement errors induced by the tip scanning over the breaking edge. These errors are also visible in other cross-sectional studies [15] and are neglected for further discussion.

Domain II represents the potential inside the top oxide layer. To evaluate the slope, a linear best fit of the potential is applied for this domain. Despite some minor variations, likely caused by the averaging effect of the tip, the linear fit resulted in a slope of 0.424.

Inside domain III, perturbations of the surface potential can arise from various sources: they are either caused by locally stored charges inside the nitride clusters or occur due to topographic crosstalk. As topographic features may be responsible for crosstalk, especially in lift mode KPFM [26], it is not possible to exclude artefacts in the measurement data of domain III. Nevertheless, the trend inside the nitride is unaffected by crosstalk, allowing for a linear connection of the measurement values from the end of the top oxide to the beginning of the bottom oxide, resulting in a slope of 0.239. In general, the slope is estimated using the ratio of the relative permittivities of the PECVD materials. With the values given in section 4, a slope ratio of 51% between the top silicon oxide and the nitride is determined, which is 0.220. Comparing the estimated and the measured values reveals that the measured value is approximately 8.5% larger than the simulated value. This might be caused by charge carriers travelling from the surface of the top oxide deeper into the multilayer, decreasing the slope in the top oxide layer. Further, the permittivity of PECVD materials can vary depending on the processing parameters [27], which emphasizes that an

Table 2. Summary of the relevant measurement data as well as coefficient of determination for domain II, domain III and domain IV.

Domain	Measured slope	Predicted slope	Relative deviation	R^2
II	0.424	0.424	—	0.998
III	0.239	0.220	8.95%	—
IV	0.462	0.424	8.54%	0.982

exclusive look at this slope cannot clearly indicate a movement of charge.

The slope inside domain IV is 0.462 and exceeds the one in the top silicon oxide layer significantly, by almost 8.9%. As both silicon oxide layers were deposited in the same PECVD process, their permittivities are the same. Taking this into account, the slopes in domain III and IV are approximately 9% steeper than expected from the measured values in domain II. Reverse calculating shows that the slope in domain II is about 9% shallower than it should be. This is a strong indicator for a movement of charge from the top silicon oxide layer to the first oxide/nitride interface and corresponds well to the simulation results in figure 7, where the slope in the top oxide is decreased after charge movement.

Table 2 summarizes the relevant calculated slopes extracted from the measurement data. Furthermore, the corrected coefficient of determination is presented. The R^2 values show that a linear fit for domain II and IV are good assumptions, whereas the topographically induced errors in domain III do not allow a direct use of the coefficient of determination. The slope of domain III was determined by connecting the measurement values 100 nm before and 100 nm after the nitride layer.

In domain V, the smooth transition between the bottom silicon oxide and the bulk silicon is not as rapid as expected from the simulation. This is due to the idealistic assumption made for the simulation, that the silicon bulk is a perfect conductor, whereas the silicon is merely highly doped. Accordingly, there are not enough free charge carriers to compensate the residual electric field at the boundary and the field is able to penetrate the silicon, resulting in a typical insulator/semiconductor transition around the bottom silicon oxide/silicon interface.

As expected, the bulk silicon in domain VI is on a constant potential, as the backside of the doped silicon is grounded. Hence, the measurement data were set to 0 V.

7. Conclusion

We presented a new atomic force microscope based method to measure the potential distribution inside negatively corona-charged ONO electrets along the z-axis. This method is especially useful for multilayers of thin materials as it is independent of material properties and has a resolution in the 10 nm range. With a combination of the KPFM method and FEM simulations, we are able to draw the first conclusions on the location of the stored charges.

FEM simulations revealed that measurements at tip distances noticeably larger than 30 nm are not able to monitor subtle variations in the potential distribution, which makes the KPFM setup a suitable method for measuring potentials in real space. The high lateral resolution of KPFM is another advantageous aspect of this method. Furthermore, theoretical considerations and simulations showed that deviations in potential distributions after thermal treatment give information on charge movement. Analysing the slope of the measured potential allowed us to show a charge movement towards the first oxide/nitride interface.

In the near future we are going to perform measurements with specialized tips such as ultra-sharp [28], nanoparticle-modified [29] or coaxial [30] tips to achieve an even higher resolution. Application of additional deconvolution algorithms as proposed by Machleidt *et al* [31] and Cohen *et al* [32] will allow us to quantify the charge densities and locations inside the materials and thus distinguish charge storage mechanisms for both polarities. Furthermore, the difference between the simulated slopes inside and outside the samples will be used for further deconvolution of the measured potential. This could give an even deeper insight into the spatial charge distribution inside the sample.

Acknowledgments

The authors want to thank Professor Dr h. c. emer. G M Sessler for the helpful discussion and the opportunity to charge and measure samples at the Technische Universität Darmstadt, Germany. We furthermore thank Germany's Free State of Bavaria for financial support from in the frame of ZeWiS.

References

[1] Amjadi H and Thielemann C 1996 Silicon-based inorganic electrets for application in micromachined devices *IEEE Trans. Dielectr. Electr. Insul.* **3** 494–8
[2] Leonov V, van Hoof C, Goedbloed M and van Schaijk R 2012 Charge injection and storage in single layer and multilayer inorganic electrets based on SiO_2 and Si_3N_4 *IEEE Trans. Dielectr. Electr. Insul.* **19** 1253–60
[3] Zhang X and Sessler G M 2001 Charge dynamics in silicon nitride/silicon oxide double layers *Appl. Phys. Lett.* **78** 2757–9
[4] Teyssedre G, Villeneuve C, Pons P, Boudou L, Makasheva K and Despax B 2012 Challenges in probing space charge at sub-micrometer scale *Annual Report of Conf. on Electrical Insulation and Dielectric Phenomena* pp 234–7
[5] Dennison J R and Pearson L H 2013 Pulsed electro-acoustic (PEA) measurements of embedded charge distributions *Proc. SPIE* **8876** 887612
[6] Fukanaga K 2008 Progress and prospects in PEA space charge measurement techniques *IEEE Electr. Insul. Mag.* **24** 26–37
[7] Hole S 2012 Behind space charge distribution measurements *IEEE Trans. Dielectr. Electr. Insul.* **19** 1208–14

[8] Zerweck U, Loppacher C, Otto T, Grafström S and Eng L 2005 Accuracy and resolution limits of kelvin probe force microscopy *Phys. Rev.* B **71** 125424
[9] Melitz W, Shen J, Kummel A C and Lee S 2011 Kelvin probe force microscopy and its application *Surf. Sci. Rep.* **66** 1–27
[10] Villeneuve-Faure C, Boudou L, Makasheva K and Teyssedre G 2014 Towards 3D charge localization by a method derived from atomic force microscopy: the electrostatic force distance curve *J. Phys. D: Appl. Phys.* **47** 455302
[11] Chang J-M, Chang W-Y, Chen F-R and Tseng F-G 2013 Direct measurement of electrostatic fields using single Teflon nanoparticle attached to AFM tip *Nanoscale Res. Lett.* **8** 519
[12] Zhang Z, Hetterich M, Lemmer U, Powalla M and Hölscher H 2013 Cross sections of operating Cu(In,Ga)Se2 thin-film solar cells under defined white light illumination analyzed by Kelvin probe force microscopy *Appl. Phys. Lett.* **102** 023903
[13] Moczała M, Sosa N, Topol A and Gotszalk T 2014 Investigation of multi-junction solar cells using electrostatic force microscopy methods *Ultramicroscopy* **141** 1–8
[14] Glatzel T, Steigert H, Sadewasser S, Klenk R and Lux-Steine M 2005 Potential distribution of Cu(In,Ga)(S,Se) 2-solar cell cross-sections measured by Kelvin probe force microscopy *Thin Solid Films* **480–481** 177–82
[15] Ankudinov A 2012 Solar cell diagnostics using Kelvin force microscopy and local photoexcitation *Microscopy Anal.* SPM Issue April pp 29–32
[16] Bergmann W, Weber S, Ramos J, Nazeeruddin M, Grätzel M, Li D, Domanska A, Lieberwirth I, Ahmad S and Berger R 2014 Real-space observation of unbalanced charge distribution inside a perovskite-sensitized solar cell *Nat. Commun.* **5** 5001
[17] Alvarez-Pampliega A, Gonzalez-Garcia Y, Van den Bergh K, De Strycker J and Terryn H 2015 Scanning Kelvin force microscopy study at the cut-edge of aluminum rich metal coated steel *Mater. Corros.* **66** 16–22
[18] Sessler G M 1998 *Electrets* vol 1 3rd edn (Morgan Hill, CA: Laplacian Press)
[19] Günther P and Sessler G M 1988 Charge storage and charge decay in silicon dioxide *Annual Report of Conf. on Electrical Insulation and Dielectric Phenomena* pp 214–9
[20] Amjadi H 1999 Investigations on charge storage and transport in plasma-deposited inorganic electrets *IEEE Trans. Dielectr. Electr. Insul.* **6** 236–41
[21] Tzeng S-D and Gwo S 2006 Charge trapping properties at silicon nitride/silicon oxide interface studied by variable-temperature electrostatic force microscopy *J. Appl. Phys.* **100** 023711
[22] Huang H, Winchester K J, Suvorova A, Lawn B R, Liu Y, Hu X Z, Hu J M, Dell J M and Faraone L 2007 Effect of deposition conditions on mechanical properties of low-temperature PECVD silicon nitride films *Mater. Sci. Eng.* A **435-436** 453–9
[23] Ahn H-S, Chizhik S A, Dubravin A M, Kazachenko V P and Popov V V 2001 Application of phase contrast imaging atomic force microscopy to tribofilms on DLC coating *Wear* **249** 617–25
[24] Rachel O 2008 Advances in AFM for the electrical characterization of semiconductors *Rep. Prog. Phys.* **71** 076501
[25] Lee M, Lee W and Prinz F 2006 Geometric artefact suppressed surface potential measurements *Nanotechnology* **17** 3728–33
[26] Barbet S, Popoff M, Diesinger H, Deresmes D, Theron D and Melin T 2014 Cross-talk artefacts in Kelvin probe force microscopy imaging: a comprehensive study *J. Appl. Phys.* **115** 144313
[27] Vogt K, Houston M, Ceiler M, Roberts C and Kohl P 1995 Improvement in dielectric properties of low temperature PECVD silicon dioxide by reaction with hydrazine *J. Electron. Mater.* **6** 751–5
[28] Zhao M, Sharma V, Wei H, Birge R, Stuart J, Papadimitra-Kopoulos V and Huey B 2008 Ultrasharp and high aspect ratio carbon nanotube atomic force microscopy probes for enhanced surface potential imaging *Nanotechnology* **19** 235704
[29] Hormeño S, Penedo M, Manzano C and Luna M 2013 Gold nanoparticle coated silicon tips for Kelvin probe force microscopy in air *Nanotechnology* **24** 395701
[30] Brown K, Satzinger K and Westervelt R 2012 High spatial resolution Kelvin probe force microscopy with coaxial probes *Nanotechnology* **23** 115703
[31] Machleidt T, Sparrer E, Kapusi D and Franke K-H 2009 Deconvolution of Kelvin probe force microscopy measurements—methodology and application *Meas. Sci. Technol.* **20** 084017
[32] Cohen C, Halpern E, Nanayakkara S U, Luther J M, Held C, Bennewitz R, Boag A and Rosenwaks Y 2013 Reconstruction of surface potential from Kelvin probe force microscopy images *Nanotechnology* **24** 295702